DELPHI Collaboration DELPHI 2002-077 CONF 611
June 30, 2002

Photon Events with Missing Energy at $\sqrt{s}$ =130 to 209 GeV.

DELPHI Collaboration

S. Ask, V. Hedberg
Lund University, Lund, Sweden
E. Anashkin, P. Checchia, A. De Min, M. Margoni, F. Mazzucato
Università e Sezione INFN, Padova, Italy
C. Matteuzzi
Università e Sezione INFN, Milano, Italy
S. Katsanevas
Université Claude Bernard de Lyon IPNL, Lyon, France
A. Perrotta
Università e Sezione INFN, Bologna, Italy

Abstract

The production of single and multi-photon events has been studied in the reaction $e^+e^- \to \gamma(\gamma) + \textit{invisible particles}$. The data collected with the DELPHI detector during the years 1999 and 2000 at centre-of-mass energies between 192 GeV and 209 GeV was combined with earlier data to search for phenomena beyond the Standard Model. The measured number of light neutrino families was three as expected and the absence of an excess of events beyond that predicted by the Standard Model processes was used to set limits on new physics. Both model independent searches and searches for new processes predicted by supersymmetric and extra-dimensional models have been made. Limits on new non-standard model interactions between neutrinos and electrons were also determined.

Contributed Paper for ICHEP 2002 (Amsterdam)

1 Introduction

The DELPHI experiment has previously reported studies of events at centre-of-mass energies up to 189 GeV with only one photon or two acoplanar photons [1, 2, 3, 4]. The other LEP experiments have reported similar studies [5]. The present paper combines all DELPHI single photon data recorded at 181-209 GeV and all acoplanar two photon data recorded at 130-209 GeV to obtain the best possible limits on new physics. The paper improves and supersedes the earlier studies made at lower energies.

At LEP2, the Standard Model predicts that events with one or more photons and invisible particles are produced exclusively by the reaction $e^+e^- \to \nu\bar{\nu}\gamma(\gamma)$ which receives a contribution from Z-exchange in the s-channel with single- or multi-photon emission from the initial state electrons and from the t-channel W exchange, with the photon(s) radiated from the beam electrons or the exchanged W. Beyond the Standard Model, contributions to the γ + *missing energy* final state could come from a new generation of neutrinos or from the radiative production of some new particle, stable or unstable, weakly interacting or decaying into a photon.

A measurement of the cross-section of the process $e^+e^- \to \nu\bar{\nu}\gamma$ determines the number of light neutrino generations, N_ν. DELPHI has previously reported measurements of N_ν using both LEPI and LEPII single photon data and this measurement has now been recalculated with all available DELPHI data.

The $e^+e^- \to \nu\bar{\nu}\gamma$ cross-section can also be used to calculate limits on new neutrino interactions with electrons, beyond what is predicted by the Standard Model. DELPHI has set bounds on the parameter space for such new neutral current interactions.

It is possible to the search for new particles as predicted by various models or in a model-independent way. The DELPHI experiment has done both. The event topology with one or two photons and missing energy can be used to look for the production of either new invisible particles tagged by initial-state radiation (ISR) or the production of invisible particles in association with a photon. The model independent single-photon searches in DELPHI take both of these possibilities into account. The first search is for the production of a new hypothetical particle tagged by an ISR-photon, $e^+e^- \to X\gamma$. The new particle, X, was in this analysis assumed to be either stable and weakly interacting or to be decaying into invisible decay products. The second model independent search consisted of looking for and setting cross section limits on the process $e^+e^- \to XY \to YY\gamma$ where X is a hypothetical new neutral particle which decays radiatively to Y which is a stable weakly interacting new neutral particle.

An example of a study in which photons are produced in association with a new particle is the search for gravitons via the process $e^+e^- \to \gamma G$. The existence of this process has been predicted by some string models [6, 7] in which gravity is allowed to propagate in a space with more dimensions than the usual four space-time dimensions.

Various theories of supersymmetry (SUSY) predict the existence of new particles which would produce final states with missing energy and one or several photons. Different assumptions about the SUSY breaking mechanism lead to two main search scenarios in which the Lightest Supersymmetric Particle (LSP) is either the gravitino ($\tilde{G}$) or the neutralino ($\tilde{\chi}_1^0$).

Gauge-Mediated Supersymmetry Breaking (GMSB) models [8] typically predict that the gravitino is the LSP with a mass less than a few hundred eV/c^2 and that the neutralino or the slepton is the Next-to-Lightest Supersymmetric Particle (NLSP). If the neutralino is

the NLSP it decays into $\tilde{G}\gamma$ with the gravitino being essentially massless and undetectable and it is possible to search for both single-photon and multi-photon production via the processes $e^+e^- \rightarrow \tilde{G}\tilde{\chi}_1^0 \rightarrow \tilde{G}\tilde{G}\gamma$ and $e^+e^- \rightarrow \tilde{\chi}_1^0\tilde{\chi}_1^0 \rightarrow \tilde{G}\gamma\tilde{G}\gamma$. The cross section for the single-photon process is proportional to $1/m_{\tilde{G}}^2$ while the two-photon process does not depend on the gravitino mass and the search for $e^+e^- \rightarrow \tilde{G}\tilde{\chi}_1^0 \rightarrow \tilde{G}\tilde{G}\gamma$ at LEP is therefore only sensitive if the gravitino is ultralight ($m_{\tilde{G}} < 10^{-4}$ eV/c^2).

If the gravitino is the LSP and it is the only supersymmetric particle which is kinematically accessible it is possible to search for $e^+e^- \rightarrow \tilde{G}\tilde{G}\gamma$ [9] by using ISR-photons to tag the undetectable production of a gravitino pair. This search makes it possible to set a lower mass limit on the gravitino mass ($m_{\tilde{G}}$) and the DELPHI collaboration has updated the calculation of this limit using all available data.

The NLSP lifetime depends on the gravitino mass and if this is sufficiently large (a few hundred eV/c^2) the neutralinos in $e^+e^- \rightarrow \tilde{\chi}_1^0\tilde{\chi}_1^0 \rightarrow \tilde{G}\gamma\tilde{G}\gamma$ will decay in such a way that the detected photons will not originate at the beam interaction point. When the mean decay paths are comparable to the detector scale, events with a single photon not pointing to the interaction region are expected and DELPHI has searched for such events.

In gravity-mediated SUSY breaking (SUGRA) models [10], the gravitino is typically heavy with a mass of several hundreds of GeV/c^2 and it is the neutralinos which are the LSP and NLSP. Under certain assumptions, $\tilde{\chi}_2^0$ will decay into a stable undetectable $\tilde{\chi}_1^0$ and a photon. This can give rise to processes such as $e^+e^- \rightarrow \tilde{\chi}_1^0\tilde{\chi}_2^0 \rightarrow \tilde{\chi}_1^0\tilde{\chi}_1^0\gamma$ and $e^+e^- \rightarrow \tilde{\chi}_2^0\tilde{\chi}_2^0 \rightarrow \tilde{\chi}_1^0\gamma\tilde{\chi}_1^0\gamma$ with both single- and two-photon production. DELPHI has searched for the two-photon process but since the predicted cross section for the single-photon process is small the previously mentioned model-independent search for $e^+e^- \rightarrow XY \rightarrow YY\gamma$ was made instead.

There exist in addition a so-called no-scale supergravity model [11] (also known as the LNZ model) in which the local supersymmetry breaking is decoupled from the global supersymmetry breaking. This results in the prediction of an ultralight gravitino and the process $e^+e^- \rightarrow \tilde{G}\tilde{\chi}_1^0 \rightarrow \tilde{G}\tilde{G}\gamma$. The main phenomenological difference between this model and the GMSB model is that only the gravitino and neutralino masses are free parameters since the selectron masses and the neutralino composition depends on the neutralino mass in the LNZ model.

This paper describes the single- and multi-photon selection criteria, the measurement of the single photon cross section and the number of neutrino families and it gives limits on non-Standard Model physics obtained from searches for gravitons in high-dimensional models and supersymmetric particles.

2 The DELPHI detector

The general criteria for the selection of events are based mainly on the electromagnetic calorimeters and the tracking system of the DELPHI detector [12]. All three major electromagnetic calorimeters in DELPHI, the High density Projection Chamber (HPC), the Forward ElectroMagnetic Calorimeter (FEMC) and the Small angle TIle Calorimeter (STIC), have been used in the single-photon reconstruction while only the FEMC and the HPC were used in the multiphoton analysis. For the study of the non-pointing single photon events only the HPC detector was used.

The barrel region of DELPHI was covered by the HPC, which was a gas sampling

calorimeter able to sample a shower nine times longitudinally. The FEMC was made up of an array of 4532 lead glass blocks in each endcap. The energy resolution of this calorimeter was degraded by the material in front of it, which caused photon conversions and even preshowers. The very forward luminosity monitor STIC [13] consisted of two cylindrical lead-scintillator calorimeters read out by wavelength-shifting fibres. Two layers of scintillators mounted on the front of each STIC calorimeter together with a smaller ringshaped scintillator mounted directly on the beampipe, provided $e-\gamma$ separation. The angular coverages of these calorimeters and the energy resolutions are given in Table 1 and the detailed characteristics and performances are described in [12].

Three different triggers were used in DELPHI to select single-photon events. The HPC trigger for purely neutral final states used a plane of scintillators inserted into one of the HPC sampling gaps at a depth of around 4.5 radiation lengths. A second level trigger decision was produced from the signals of analog electronics and was based on a coincidence pattern inside the HPC module. The trigger efficiency has been measured with Compton and Bhabha events. It was strongly dependent on the photon energy, E_γ, rising steeply up to ∼12 GeV, with about 30% efficiency at 4 GeV and above 80% when $E_\gamma > 30$ GeV. It reached a maximum of 87% at $E_\gamma \simeq E_{\rm beam}$. This efficiency does not include losses due to the cracks between modules of the HPC detector. The FEMC trigger required an energy deposition of at least 2.5 GeV. The efficiency increased with energy and was ∼97% at 18 GeV. Correlated noise in several adjacent channels caused fake triggers, but these could be rejected offline with high efficiency by algorithms that took into account the lead glass shower pattern. The STIC trigger required an energy deposition of at least 15 GeV and reached maximum efficiency at 30 GeV. The trigger efficiency has been measured with samples of photons from $e^+e^-\gamma$ and $q\bar{q}\gamma$ events. The efficiency varied between 74% and 27% over the angular region used in the analysis.

In addition to the electromagnetic calorimeters, the DELPHI tracking system was used to reject events in which charged particles were produced. The main tracking devices were the Time Projection Chamber (TPC) and the microVertex silicon Detector (VD) and its extension into the forward region, the Very Forward Tracker (VFT). The silicon trackers were also used for electron/photon separation by vetoing photon candidates which could be associated with hits in these detectors.

Finally, the Hadron CALorimeter (HCAL) and its cathode-read-out system were used to reject cosmic rays and to provide photon/hadron separation, while the DELPHI Hermeticity Taggers were used to ensure complete detector hermeticity for additional neutral particles.

3 Event selection

3.1 Single-photon events

The single photon events were selected in two stages. In the first stage, all events with one photon were preselected and compared to the Standard Model process $e^+e^- \to \nu\bar{\nu}\gamma$. These events were also used to calculate cross-sections and for a determination of the number of light neutrino families. A likelihood ratio method was then used to maximize the sensitivity in the various single photon searches.

3.1.1 Preselection

Different analyses were made depending on in which of the three electromagnetic calorimeters the photon candidate was found:

- Events with a photon in the HPC were selected by requiring a shower having a scaled energy $x_\gamma = E_\gamma/E_{beam} > 0.06$ and a polar angle, θ, between 45° and 135° and no charged particle tracks. Electronic noise and alpha particles emitted from the lead converter created fake low-energy showers in the HPC but these could be rejected very effectively by requiring the longitudinal shower profile to satisfy conditions defining a good electromagnetic shape [1]. Background from radiative Bhabha events and Compton events were rejected by requiring no other electromagnetic showers in the event unless they were in the HPC and within 20° of the first one. Cosmic rays were rejected mainly by the hadron calorimeter. If there were two or more hadronic showers the event was discarded and if only one HCAL shower was present, the event was rejected if the shower was not consistent with being caused by punch-through of the electromagnetic shower. A constraint on the γ direction was imposed, requiring that the line of flight from the mean interaction point and the shower direction measured in the calorimeter coincided within 15°. Also the requirement of no charged particles removed cosmic ray background.

  The photon identification efficiency was determined on the basis of a Monte Carlo sample of events passed through the complete simulation of the DELPHI detector [14]. The efficiency depended on the photon energy and it ranged from ∼45% at 6 GeV to ∼71% for $E_\gamma > 15$ GeV.

- Events with at least one shower in the FEMC with a scaled energy $x_\gamma > 0.10$ and a polar angle in the intervals $12° < \theta < 32°$ or $148° < \theta < 168°$ were selected. The large background of radiative Bhabha events made it necessary to add an energy-dependant angular requirement, $\theta > 28° - 80° \cdot x_\gamma$, which only affected the very low energy region $x_\gamma < 0.20$. In order to separate electrons from photons, the FEMC shower was extrapolated to the interaction point and the event was rejected if hits in the silicon microvertex detectors (VD and VFT) could be associated with the shower. The showers in the inner and outer radial parts of the FEMC were discarded because of the large amount of material (about $2X_0$) in front of the FEMC due to the STIC and the TPC detectors. The material in front of the FEMC meant that about half of the photons preshowered before reaching the calorimeter. Most of the preshower was contained in a cone of about 15° around the largest shower and the selection took this into account by requiring no charged particle tracks, no other electromagnetic showers and no hadronic showers outside a 15° cone. If there were no charged particle tracks inside the cone either, i.e., the photon had not preshowered, it was required that only one FEMC shower was present in the event. If, on the other hand, charged particle tracks were present in the cone, more FEMC showers were allowed and their momentum vectors were added to that of the largest shower. The requirement of no electromagnetic showers outside the cone greatly reduced the background of radiative Bhabha and Compton events by rejecting events that had one or both electrons in the acceptance of the experiment. Events due to cosmic rays were rejected by the requirement of no hadronic showers

outside the cone. Inside the cone, hadronic energy was allowed only in the first layer of the HCAL.

Most reconstruction and event selection efficiencies in the analysis were taken into account by using Monte Carlo samples passed through the extensive detector simulation package of DELPHI [14]. Some efficiencies, however, were determined from data. In particular, the requirements of no electromagnetic or hadronic showers and no charged particles were studied. A sample of events triggered at random and a sample of back-to-back Bhabha events with the electrons in the STIC were used for this purpose. It was found that noise and machine background caused showers and tracks which would veto about 14% of the good single-photon events.

- Single photons in the STIC were preselected by requiring one shower with a scaled energy $x_\gamma > 0.30$ and with $3.8^\circ < \theta < 8^\circ$ or $172^\circ < \theta < 176.2^\circ$. The large background coming from beam-gas interactions made it necessary to add an energy-dependant angular requirement, $\theta > 9.2^\circ - 9^\circ \cdot x_\gamma$, which only affected the low energy region $x_\gamma < 0.60$. It was furthermore required that there were no other electromagnetic showers, no hadronic showers and no charged particles in the event. All single-photon candidates had to satisfy the STIC single-photon trigger and it was required that there was no signal in at least one of the two scintillator planes in front of the shower. A requirement of no signal in the small scintillators mounted on the beampipe made it possible to reject radiative $ee\gamma$ background.

  The trigger efficiency in the STIC acceptance was discussed in Section 2. The offline photon identification and reconstruction resulted in an additional loss of 5% of the photons. The selection of events with no shower in the STIC and no tracks implied similar losses to those found in the FEMC analysis and were estimated with the same methods.

3.1.2 Final selection

A likelihood ratio method was used to select the final sample of events in the various searches using single photon events. The photon energy was used as the final discriminating variable and two likelihood functions ($f_S(E_\gamma)$ and $f_B(E_\gamma)$) were produced from the normalized photon energy distributions of the simulated signal and background events, after passing trough the same selection criteria. The likelihood ratio function was defined as $\mathcal{L}_R = f_S(E_\gamma)/f_B(E_\gamma)$ where an event with $\mathcal{L}_R > \mathcal{L}_R^{CUT}$ was selected as a candidate event. The value of $\mathcal{L}_R^{CUT}$ was optimized to give the minimum signal cross section excluded at 95% C.L. in the absence of a signal:

$$\sigma^{min}(\mathcal{L}_R^{CUT}) = \frac{N_{95}^{min}(\mathcal{L}_R^{CUT})}{\epsilon^{max}(\mathcal{L}_R^{CUT}) \times L}$$

where N_{95}^{min} is the upper limit on the number of signal events at 95% C.L., ϵ^{max} is the efficiency for the signal and L is the luminosity. This method optimizes the background suppression for a given signal efficiency [15]. A more detailed description of the method can be found in [16].

3.2 Multi-photon events

Multi-photon events were selected by a two-step procedure. In the first preselection step, events with two photons and missing energy were selected. This sample was dominated by the Standard Model process $e^+e^- \to \nu\bar{\nu}\gamma\gamma(\gamma)$ and it was used to monitor the modelling of the $e^+e^- \to \nu\nu\gamma\gamma(\gamma)$ process by the KORALZ 4.02 generator [17]. In a second step, the selection criteria were tightened in order to improve the experimental sensitivity for possible signals of supersymmetry, such as the $e^+e^- \to \tilde{\chi}_1^0\tilde{\chi}_1^0 \to \tilde{G}\gamma\tilde{G}\gamma$ or $e^+e^- \to \tilde{\chi}_2^0\tilde{\chi}_2^0 \to \tilde{\chi}_1^0\gamma\tilde{\chi}_1^0\gamma$ processes. This was achieved by imposing more stringent requirements on the photon polar angles as well as on the event missing mass and transverse momentum.

3.2.1 Preselection

The preselection required that there was at least two electromagnetic clusters in the HPC and FEMC detectors with $x_\gamma > 0.05$ and that the event had a total visible energy $E_{vis} < 0.9\sqrt{s}$ and a total transverse momentum $p_T > 0.03E_{miss}$ where $E_{miss} = \sqrt{s} - E_{vis}$. The polar angle of the clusters was required to be in the region $10^\circ < \theta < 170^\circ$ with at least one cluster in $25^\circ < \theta < 155^\circ$. The clusters were identified as photons by requiring that there were no reconstructed charged particle tracks and no hits in the VD or VFT detectors that could be associated with the clusters.

All small FEMC and HPC showers in a cone of 10° around the main shower were merged together. Noise and clusters from alpha particles were rejected by requirements on the longitudinal shower profile [3] and the reconstructed shower axis had to point to the interaction point within 25°.

In order to reduce the background from $e^+e^- \to \gamma\gamma$ events it was required that the acoplanarity was greater than 3°. A requirement of no hits in the Hermeticity Taggers reduced the background of $e^+e^- \to \gamma\gamma\gamma$ where one photon was lost in the cracks between the calorimeters. By requiring that the acoplanarity was less than 140° when $|\theta_{\gamma 1} - \theta_{\gamma 2}| < 20^\circ$ it was possible to eliminate single photon events with the photon converting in the material in front of the calorimeters and producing two separate clusters. Cosmic events were rejected by vetoing on energy deposits in the external layers of the HAC. Doubly radiative Bhabha events where the electrons escape detection along the beampipe could be rejected by requiring that the energy in STIC was less than $0.02\sqrt{s}$ and that the polar angle of the missing momentum was in the region $10^\circ < \theta_{miss} < 170^\circ$.

If the events had three electromagnetic clusters passing the previous selection it was retained if it had $E_{vis} < 0.8\sqrt{s}$ and the sum of the angles of the three observed photons was less than 358°, i.e., if the event was significantly aplanar. Events with four or more electromagnetic clusters were discarded.

3.2.2 Final selection

The final selection in the search for $e^+e^- \to \tilde{\chi}_1^0\tilde{\chi}_1^0 \to \tilde{G}\gamma\tilde{G}\gamma$ required that the scaled transverse momentum for each cluster satisfied $p_{T\gamma}/E_{beam} > 0.07$ if the missing mass (M_{miss}) was larger than 60 GeV/c^2 and $p_{T\gamma}/E_{beam} > 0.14$ if $80 < M_{miss} < 110$ GeV/c^2. This requirement strongly suppressed the Standard Model background coming from $e^+e^- \to \nu\nu\gamma\gamma(\gamma)$ where the photons, being emitted from the initial state particles, have a relatively low transverse momentum. The more stringent requirement was used when the missing mass was close to the Z mass and the background was larger. It was in addition

required that the energies and angles of the detected photons were compatible with those expected for a particular $\tilde{\chi}_1^0$ mass.

In the search for $e^+e^- \to \tilde{\chi}_2^0\tilde{\chi}_2^0 \to \tilde{\chi}_1^0\gamma\tilde{\chi}_1^0\gamma$, the cut on transverse momentum was exchanged for a cut on the polar angle of the photons. It was required that $20^\circ < \theta_\gamma < 160^\circ$ if $M_{miss} > 60$ GeV/c^2 and $40^\circ < \theta_\gamma < 140^\circ$ if $80 < M_{miss} < 110$ GeV/c^2. The energies of the detected photons had to be compatible with those expected for a particular pair of $\tilde{\chi}_1^0$ and $\tilde{\chi}_2^0$ masses.

The efficiency of the selection was studied using simulated $e^+e^- \to \tilde{\chi}_1^0\tilde{\chi}_1^0 \to \tilde{G}\gamma\tilde{G}\gamma$ and $e^+e^- \to \tilde{\chi}_2^0\tilde{\chi}_2^0 \to \tilde{\chi}_1^0\gamma\tilde{\chi}_1^0\gamma$ events. The estimated efficiency was in the range 40-55% for both search scenarios [3].

3.3 Non-pointing single-photon events

The fine granularity of the HPC calorimeter provided a precise reconstruction of the axis direction in electromagnetic showers. This feature was used to select events with a single photon whose flight direction did not point to the beam interaction region. Events with a single non-pointing photon are expected when two neutral particles with large mean decay paths (> 4 m) are produced which subsequently decay into a photon and an invisible particle since the probability that both photons are recorded is then small.

Events of this kind were searched for by requiring one photon in the HPC calorimeter with $E_\gamma > 10$ GeV and an impact parameter exceeding 40 cm. A more stringent HPC cluster selection was made compared to the multi-photons selection [3]. This was done in order to reject noise and cosmic events which was a larger problem in the non-pointing single photon analysis.

It was required that the events had no reconstructed tracks and that no hits in the vertex detector could be associated with the electromagnetic shower. Cosmic ray events, which represented the main experimental background, were largely reduced by vetoing on isolated hits or tracks in the Hermeticity Taggers and signals from the external HCAL layers and from the cathode-read-out system of the hadron calorimeter.

The efficiency of the selection was studied using simulated $e^+e^- \to \tilde{\chi}_1^0\tilde{\chi}_1^0 \to \tilde{G}\gamma\tilde{G}\gamma$ events that had passed through the entire DELPHI detector simulation package. For a mean decay path of 3-8 m the efficiency was 4-5% [3].

4 Real data and simulated samples

4.1 Data samples

The ten data samples that were used in the single photon analysis are summarized in Table 2. These samples were recorded by DELPHI during 1997 to 2000. The multi photon analysis also included data recorded during 1995 and 1996 at the centre-of-mass energies of 130, 136, 161 and 172 GeV. These samples added another 21 pb^{-1} of luminosity.

4.2 Simulation of background and signal

4.2.1 The single photon analysis

Apart from the $e^+e^- \to \nu\bar{\nu}\gamma(\gamma)$ process, single-photon events can be faked by the QED reaction $e^+e^- \to e^+e^-\gamma$ if the two electrons escape undetected along the beampipe or if the electrons are in the detector acceptance but are not detected by the experiment.

This process has a very high cross-section, decreasing rapidly when the energy (E_γ) and the polar angle (θ_γ) of the photon increase. The behaviour of this QED background together with the rapidly varying efficiencies at low energies are the reasons why different energy cuts had to be applied to photons in the three calorimeters: $x_\gamma > 0.06$ (HPC), $x_\gamma > 0.10$ (FEMC) and $x_\gamma > 0.30$ (STIC). The energy dependent cut on the polar angle in the FEMC and STIC analysis were also necessary to reduce this background. Another critical parameter in the rejection was the polar angle at which the electrons start being seen in the STIC detector. This detector reconstructs electrons down to $\theta = 2.2°$ and in addition, the scintillator counters mounted on the beampipe could be used to reject events with electrons down to 1.8°. Simulations have shown that even at lower angles (down to 0.97°) a large fraction of the electrons were detectable because they interacted with a tungsten shield mounted inside the beampipe and leaked enough energy into the STIC to make it possible to reject the events.

The remaining background from the $e^+e^-\gamma$ process was calculated with a Monte Carlo program [18] and two different event topologies were observed. Either both electrons were below the STIC acceptance or one of the electrons was in the DELPHI acceptance where it was wrongly identified as a photon, and the photon was lost in the cracks between the electromagnetic calorimeters. The first topology gives background at low photon energy while the second one produces fake photon events at high energy.

In the STIC analysis, an additional background was the single electrons produced by interactions between the beam particles and residual gas molecules in the LEP beampipe. In these $e \to e\gamma$ events the photons were always lost in the beampipe while the off-energy electrons were bent into the STIC acceptance by the low-beta quadrupoles close to DELPHI. The rate of this background was so large that it was not possible to provide a $\gamma - e$ separation powerful enough to eliminate this background completely. A simulation has been made of off-energy electron production [19], but it could not be used in the analysis since the vacuum pressure around the LEP ring was not known to the required precision. Instead, a background sample was collected with a trigger similar to the photon trigger except that it did not use the scintillators for photon-electron separation. After applying all the cuts used in the single photon analysis, except the scintillator requirements, this background sample was used to estimate the remaining off-energy electron background.

The contribution from other processes such as $\gamma\gamma$ collisions, $e^+e^- \to \gamma\gamma\gamma$, cosmic ray events, $e^+e^- \to \mu^+\mu^-\gamma$ and $e^+e^- \to \tau^+\tau^-\gamma$ has also been calculated.

The $\nu\bar{\nu}\gamma(\gamma)$ process was simulated by the KORALZ [17] program. Comparisons of the predicted total cross section from KORALZ with that of the NUNUGPV [20] program showed a good agreement while there were some differences in the differential cross-sections.

4.2.2 The multi photon analysis

Multi-photon final states can be produced at LEP via the reactions $e^+e^- \to \nu\bar{\nu}\gamma\gamma(\gamma)$ and $e^+e^- \to \gamma\gamma(\gamma)$. In the case of double ISR with final state $\nu\bar{\nu}$ production, the photons tend to have a relatively low transverse momentum and tend to have both large acoplanarity and large acollinearity. Since the neutrino production is mainly mediated by Z-exchange in the s-channel, the missing mass distribution have a large peak corresponding to the mass of the Z. The $e^+e^- \to \nu\bar{\nu}\gamma\gamma(\gamma)$ process was, as in the single photon case, simulated by the KORALZ generator [17].

The process $e^+e^- \to \gamma\gamma(\gamma)$ is a QED interaction between the incoming electrons and it is mediated by an electron in the t-channel. The RADCOR model [21] was used to simulate this background. The process is easy to reject when only two hard photons are produced but if additional hard ISR photons are emitted and lost in the beampipe, the visible photon pair can show relatively large acollinearity but small acoplanarity.

Additional minor background contributions can come from double radiative Bhabha events $e^+e^- \to e^+e^-\gamma\gamma$ when one or two electrons remain undetected or are wrongly identified as photons. The BABAMC program [22] was used as an event generator for these events. A requirement of a minimum transverse missing momentum very effectively eliminated the cases where both electrons escaped along the beampipe.

5 Comparison with the Standard Model expectations

5.1 Single-photon cross-section

The energy spectrum of the 1526 selected single photon events from all calorimeters is shown in Figure 1 together with the expected contributions from known sources. The X_γ distributions are shown for three $\sqrt{s}$-bins and the luminosity and average $\sqrt{s}$ of the datasets that make up these bins are given in Table 2. The $\nu\bar{\nu}\gamma$ process was simulated by the KORALZ [17] program and then passed through the extensive detector simulation package of DELPHI [14]. The single-photon event selection was such that events with more than one photon could survive if the other photons were at low angle ($\theta_\gamma < 2.2°$), low energy ($E_\gamma < 0.8$ GeV) or within 3°, 15° and 20° from the highest energy photon in the STIC, FEMC and HPC respectively.

The missing mass (or recoil mass) distributions of the events recorded at $\sqrt{s}$=181-209 GeV are shown in Figure 2. In this plot the distributions obtained with each of the three DELPHI electromagnetic calorimeters are shown separately. No sign of an excess above the Standard Model expectation is seen in either the highest energy data nor in any of the three calorimeter analysis.

The number of events and cross-sections obtained from the event samples after correcting for background and efficiencies are given in Table 3. This table does not include the FEMC events with $x_\gamma < 0.20$ since they were only used in the searches and not in the cross-section calculations. The previously mentioned Monte Carlo programs were used to calculate the expected values of the cross-section of the process $e^+e^- \to \nu\bar{\nu}\gamma(\gamma)$ inside the acceptance of each of the three detectors used in the analysis. The contributions from various sources to the systematic error in the cross-section measurement are given in Table 4. The dominant uncertainty comes from the estimation of trigger and detection efficiencies. The calculation of the expected cross-section has a theoretical uncertainty

which is approaching 1% with the latest versions of KORALZ [17] and this error is thus insignificant compared with the experimental systematic errors.

Figure 3 shows the expected behaviour of the Standard Model single photon cross-section as a function of the LEP energy, compared with the values measured with all three DELPHI calorimeters. The impression from this plot is that the data is below the Standard Model expectation calculated by KORALZ but this difference is not statistically significant.

5.2 Non-pointing single-photon events and multi-photon events

The numbers of events with a single non-pointing photon or with multi-photon final states are compared to Standard Model expectations in Table 5.

The missing mass spectra for the preselected multi-photon events and the expected contribution from $e^+e^- \to \nu\overline{\nu}\gamma\gamma(\gamma)$ as simulated with KORALZ are shown in Figure 4. Additional background contributions from the processes $e^+e^- \to e^+e^-\gamma$ and $e^+e^- \to \gamma\gamma\gamma$ have been estimated to be 0.43±0.16 events at the preselection level and have been added to the simulated sample. The measured missing mass distribution is in good agreement with the simulation and no significant excess over Standard Model expectations was found in any of the data samples collected at energies up to $\sqrt{s} = 209$ GeV.

6 Limits on new phenomena

6.1 Neutrino physics

6.1.1 Measurement of the number of light neutrino families

A measurement of the cross-section of the process $e^+e^- \to \nu\bar{\nu}\gamma$ determines the number of light neutrino generations, N_ν. The LEP2 cross-section measurements have been compared with the expected cross sections for 2, 3 and 4 neutrino generations, calculated with KORALZ, and the number of neutrino generations has been deduced (Table 3). Averaging the independent measurements from the three different calorimeters at $\sqrt{s} = 181 - 209$ GeV, the number of light neutrino generations becomes:

$$N_\nu = 2.80 \pm 0.10(stat) \pm 0.14(syst)$$

6.1.2 Neutrino interactions beyond the Standard Model

Calculations of the contribution to the single photon process $e^+e^- \to \nu\bar{\nu}\gamma$ from Non-Standard (NS) neutrino interactions with the electron have recently been made to study theories which are candidates to explain the solar and atmospheric neutrino anomalies [23]. The single photon cross-section contribution from the NS neutrino interactions was computed at tree level in a point interaction approximation where $\epsilon_{\alpha R}$ and $\epsilon_{\alpha L}$ $(\alpha = e, \mu, \tau)$ parametrize the strength of the non standard interactions between the three neutrinos and the electron, relative to the Fermi constant (G_F). The radiator approximation was used in these calculations to determine the single photon cross section from initial state radiation.

The analysis was made for three different assumptions as suggested by [23]:

I. The NS interactions only couple to the electron neutrino, $e^+e^- \to \nu_e\nu_e\gamma$.

II. The NS interactions only couple to the tau neutrino, $e^+e^- \to \nu_\tau\nu_\tau\gamma$.

III. The NS interactions only couple to a flavor changing neutral current, $e^+e^- \to \nu_\alpha\nu_\beta\gamma$ where $\alpha \neq \beta$.

In all three cases, the analysis was based on the single photon samples recorded with the HPC and FEMC detectors and the event selection was optimized with a likelihood ratio method. Under the first assumption, the interference terms between the NS interaction and the SM amplitudes can, in some parts of the $\epsilon_{eL} - \epsilon_{eR}$ parameter space, give a negative contribution to the single photon cross-section at a level which the analysis is sensitive enough to exclude. For this reason, the analysis under the first assumption, was divided into two independent parts based on the regions of the photon energy distribution with a positive and negative contribution from NS neutrino interactions.

The excluded regions in the $\epsilon_L - \epsilon_R$ planes for the three different assumptions are shown in Figure 5. To exclude a point in the $\epsilon_{eL} - \epsilon_{eR}$ plane a logical OR was used between the two analysis of positive and negative interference and this gives the "half moon" shape of the non-excluded region in Figure 5a. All limits are made at a 95% C.L. and the limits are computed by a bayesian multichannel method using the data collected with $\sqrt{s}$ = 200-209 GeV.

6.2 Limits on the production of unknown neutral states

6.2.1 Limits on $e^+e^- \to X\gamma$ production

The observed single photon events have been used to set a limit on the production cross-section of a new hypothetical particle, X, produced in association with an ISR photon and being stable or decaying to invisible decay products. Limits are calculated from the missing mass distribution (Figure 6) at $\sqrt{s} = 200 - 209$ GeV (average $\sqrt{s}$ =205.4 GeV) of the 414 single γ events in the angular region $12^\circ - 168^\circ$ and the 190 events in the angular region $45^\circ - 135^\circ$ while taking into account the expected background. The limit is valid when the intrinsic width of the X particle is negligible compared to the detector resolution (the recoil mass resolution varies between 10 GeV at the Z^0 peak to 1 GeV at high masses). The upper limit at the 95% confidence level of the cross-section for $e^+e^- \to \gamma$+X is given in Figure 6 for photons in the HPC region and in the FEMC+HPC region. In the latter case an assumption of an ISR-like photon angular distribution has been made to correct for losses between the calorimeters.

6.2.2 Limits on $e^+e^- \to XY \to YY\gamma$ production

A cross-section limit has been calculated for the scenario where hypothetical X- and Y-particles are produced and the X-particle decays into a Y and a photon, $e^+e^- \to XY \to YY\gamma$. It is assumed that the Y particles escapes detection (such as in the process $e^+e^- \to \tilde{\chi}_2^0\tilde{\chi}_1^0 \to \tilde{\chi}_1^0\tilde{\chi}_1^0\gamma$ which is predicted by certain SUSY models) and that the branching ratio of $X \to Y\gamma$ is 100% .

It is, in addition, assumed that the E_γ- and $cos(\theta_\gamma)$-distributions are flat. This assumption results in a very small predicted signal within the STIC acceptance and for this reason only the single photon events recorded by the HPC and FEMC detectors were used

in this analysis. Only the highest $\sqrt{s}$-bin (200-209 GeV) was used in the analysis and it was assumed that any $\sqrt{s}$-dependence of the signal would be insignificant in this limited $\sqrt{s}$-range. The analysis has been performed at 401 points in the mass plane of the X and Y particles where the selection cuts have been optimized in every point with a likelihood ratio method. The obtained and expected cross-section limits, within the HPC + FEMC acceptance, in the mass plane of the X and Y particles are shown in Figure 7.

6.3 Limits on the production of gravitons

If there are extra compact dimensions of space in which only gravity can propagate, gravitational interactions could be unified with gauge interactions already at the weak scale [6, 7]. The consequence of this model is that at LEP gravity could manifest itself by the production of gravitons (G), which themselves would be undetectable by the experiments. Instead single photons from the $e^+e^- \to \gamma G$ reaction are observable.

In these gravitational models, a fundamental mass scale, M_D, is introduced, which is related to the gravitational constant, the size of the compactified space and the number of dimensions, n, in addition to the usual 4 dimensional space. The differential cross-section for the $e^+e^- \to \gamma G$ process has been calculated by [7].

From Figure 2 it is clear that a very small signal can be expected in the STIC detector compared with the one in the FEMC and the HPC. For this reason only the two latter detectors were used in this analysis. All DELPHI data with $\sqrt{s} > 181$ GeV was used and for each bin in $\sqrt{s}$ (see Table 2) a limit was calculated after a cut optimization based on a likelihood ratio method [25]. These limits were then combined to give a cross-section limit at 95% C.L. and at 208 GeV of 0.14 pb for 2 and 4 extra dimensions. The resulting limits on the fundamental mass scale are $M_D > 1.36$ TeV for n=2 and $M_D > 0.84$ TeV for n=4 (Figure 8). This in turn translates into a limit on the size (radius) of the extra dimensions wich is $R < 0.26$ mm and $R < 13$ pm for 2 and 4 extra dimensions. Limits for other numbers of extra dimensions are given in Table 6.

6.4 SUSY particles

6.4.1 Limits on the gravitino mass

The cross-section for the process $e^+e^- \to \tilde{G}\tilde{G}\gamma$ has been computed under the assumption that all other supersymmetric particles are too heavy to be produced [9] and lower limits on the mass of such a light gravitino has been extracted previously at LEP [5, 4]. The largest sensitivity is obtained with photons at low energy and/or low polar angle. Since the signal cross-section grows as the sixth power of the center-of-mass energy, the highest sensitivity is also found at the highest available beam energy.

After a combination in the same fashion as in the graviton analysis, a limit of $\sigma <$ 0.18 pb at 95% C.L. and at 208 GeV was obtained by using the data at $\sqrt{s} = 181{-}209$ GeV from the FEMC and the HPC detectors. This corresponds to a lower limit on the gravitino mass which is

$$m_{\tilde{G}} > 1.12 \cdot 10^{-5} \text{ eV/c}^2 \quad \text{at 95\% C.L.}$$

while the expected limit is $1.14 \cdot 10^{-5}$ eV/c^2. Since the supersymmetry-breaking scale $|F|^{\frac{1}{2}}$ is related to the gravitino mass and the gravitational constant (G_N) by $|F| = \sqrt{\frac{3}{8\pi}/G_N} \cdot m_{\tilde{G}}$, the limit on this scale is $|F|^{\frac{1}{2}} > 217$ GeV.

6.4.2 Limits on neutralino production if $\tilde{G}$ is the LSP

Supersymmetric models such as the gauge-mediated supersymmetric (GMSB) model [8] or the "no-scale" supergravity model (also known as the LNZ model) [11] predict that the gravitino $\tilde{G}$ is the lightest supersymmetric particle (LSP). If the next-to-lightest supersymmetric particle (NLSP) is the neutralino $\tilde{\chi}_1^0$, both single-photon and multi-photon production can occur at LEP2 via the processes $e^+e^- \rightarrow \tilde{G}\tilde{\chi}_1^0 \rightarrow \tilde{G}\tilde{G}\gamma$ and $e^+e^- \rightarrow \tilde{\chi}_1^0\tilde{\chi}_1^0 \rightarrow \tilde{G}\gamma\tilde{G}\gamma$. While the rate of the former process is proportional to the inverse of the gravitino mass squared, the di-photon process is independent of the gravitino mass. Consequently, the single-photon process is expected to dominate only for ultra light gravitinos.

The expected photon distributions from the process $e^+e^- \rightarrow \tilde{G}\tilde{\chi}_1^0 \rightarrow \tilde{G}\tilde{G}\gamma$ were generated with SUSYGEN [24], and the event selection was optimized with a likelihood ratio method. The same analysis was repeated at 26 different neutralino masses ($m_{\tilde{\chi}_1^0}$) between 80 and 208 GeV. The cross section limit for $e^+e^- \rightarrow \tilde{G}\tilde{\chi}_1^0 \rightarrow \tilde{G}\tilde{G}\gamma$ production was computed at 208 GeV and at a 95% C.L. after combining the limits from the the single photon data recorded with the FEMC and HPC detectors at a $\sqrt{s}$ between 181 and 209 GeV, assuming the signal cross-section to scale as β^8 (where β is the neutralino velocity).

The analysis was applied to two different theoretical scenarios. The first one was a more general scenario where the neutralino was assumed to be a pure bino and the right- and left-handed selectrons were degenerated in mass. Figure 9 shows the cross section limit within the FEMC + HPC acceptance assuming that the branching ratio $Br(\tilde{\chi}_1^0 \rightarrow \tilde{G}\gamma) =$ 100% . The exclusion regions in the $m_{\tilde{\chi}_1^0}$-$m_{\tilde{G}}$ mass plane are also depicted in Figure 9 for the selectron masses $m_{\tilde{e}} = 75$ GeV and $m_{\tilde{e}} = 150$ GeV.

The second scenario was the previously mentioned "no-scale" supergravity model where the selectron masses and the neutralino composition depend on the neutralino mass. This model also predicts a very light gravitino and the cross section limit and the exclusion region in the $m_{\tilde{\chi}_1^0}$ versus $m_{\tilde{G}}$ mass plane for this model can also be seen in Figure 9.

In the search for $e^+e^- \rightarrow \tilde{\chi}_1^0\tilde{\chi}_1^0 \rightarrow \tilde{G}\gamma\tilde{G}\gamma$ at $\sqrt{s}$ =204-209 GeV, 8 events were observed with 7.3 expected from Standard Model sources. This brings the total number of events found at $\sqrt{s}$ =130-209 GeV to 24 with 21 expected (Table 5). Figure 10 shows the cross-section limit [25] calculated from these events as a function of the $\tilde{\chi}_1^0$ mass (assuming a branching ratio of 100% for $\tilde{\chi}_1^0 \rightarrow \tilde{G}\gamma$) and the exclusion region in the $m_{\tilde{\chi}}$ versus $m_{\tilde{e}_R}$ plane. The dependence of the signal cross-section on the selectron mass is due to the possibility of t-channel selectron exchange in the production mechanism. As shown in Figure 10, a lower limit of 96 GeV/c^2 (100 GeV/c^2) at 95% C.L. for the χ_1^0 mass can be deduced with the hypotheses $m_{\tilde{e}_R} = m_{\tilde{e}_L} = 2m_{\tilde{\chi}}$ ($m_{\tilde{e}_R} = m_{\tilde{e}_L} = 1.1m_{\tilde{\chi}}$) and $\chi_1^0 \approx \tilde{B}$.

If the gravitino mass is larger than 200-300 eV/c^2, the $\tilde{\chi}_1^0$ can have such a long lifetime that it will decay far from the production point yet within the detector. The signature for this case is photons that do not point to the interaction region. If the decay length is long, the probability to detect both photons is small and therefore single photon events were searched for which had a shower axis reconstructed in the HPC which gave a beam crossing point at least 40 cm away from the interaction point. 5 events were found at 202-209 GeV with 3 expected, bringing the total at all energies to 16 with 15 expected from Standard Model sources (Table 5).

Figure 11 shows the cross-section limit as a function of the mean decay path of the

neutralino from the non-pointing single photon events.

6.4.3 Limits on neutralino production if $\tilde{\chi}_1^0$ is the LSP

In other SUSY models [10] the $\tilde{\chi}_1^0$ is the LSP and $\tilde{\chi}_2^0$ is the NLSP. The $e^+e^- \to \tilde{\chi}_2^0\tilde{\chi}_2^0 \to \tilde{\chi}_1^0\gamma\tilde{\chi}_1^0\gamma$ process has an experimental signature which is the same as for $e^+e^- \to \tilde{\chi}_1^0\tilde{\chi}_1^0 \to \tilde{G}\gamma\tilde{G}\gamma$ but with somewhat different kinematics due to the masses of the $\tilde{\chi}_1^0$ and $\tilde{\chi}_2^0$. The previous DELPHI analysis at lower energies [4, 3] has now been repeated with the 204-209 GeV data sample. Nine events remain after all cuts, with 8 expected from the Standard Model background (Table 5). The total number of events found at $\sqrt{s}$ =130-209 GeV was 26 with 24 expected. Figure 12 shows the observed and expected cross-section limit calculated from the events collected at all energies as a function of the $\tilde{\chi}_1^0$ and $\tilde{\chi}_2^0$ masses, assuming a branching ratio of 100% for $\tilde{\chi}_2^0 \to \tilde{\chi}_1^0\gamma$.

7 Conclusions

The DELPHI experiment has analysed all single- and acoplanar multi-photon events collected during 1995-2000 at a center-of-mass energy between 130-209 GeV.

The measured single and multi photon cross-section is in agreement with the expectations from the Standard Model process $e^+e^- \to \nu\bar{\nu}\gamma(\gamma)$.

The absence of an excess of events has been used to set limits on the production of new unknown model-independent neutral states, a light gravitino and neutralinos.

A new limit on the gravitational scale and on non-standard model interactions have also been determined.

References

[1] DELPHI Collaboration, P. Abreu *et al.*, Phys. Lett. **B380** (1996) 471.

[2] DELPHI Collaboration, P. Abreu *et al.*, Eur. Phys. J. **C1** (1998) 1.

[3] DELPHI Collaboration, P. Abreu *et al.*, Eur. Phys. J. **C6** (1999) 371.

[4] DELPHI Collaboration, P. Abreu *et al.*, Eur. Phys. J. **C17** (2000) 53.

[5] ALEPH Collaboration, R. Barate *et al.*, Phys. Lett. **B420** (1998) 127;
ALEPH Collaboration, R. Barate *et al.*, Phys. Lett. **B429** (1998) 201;
L3 Collaboration, M. Acciarri *et al.*, Phys. Lett. **B411** (1997) 373;
L3 Collaboration, M. Acciarri *et al.*, Phys. Lett. **B444** (1998) 503;
OPAL Collaboration, K. Ackerstaff *et al.*, Eur. Phys. J. **C2** (1998) 607;
OPAL Collaboration, K. Ackerstaff *et al.*, Eur. Phys. J. **C8** (1999) 23.

[6] N. Arkani-Hamed, S. Dimopoulos and G. Dvali, Phys. Lett. **B429** (1998) 263.
E.A. Mirabelli, M. Perelstein and M.E. Peskin, Phys. Rev. Lett. **82** (1999) 2236.

[7] G.F. Giudice, R. Rattazzi and J.D. Wells, Nucl. Phys. **B544** (1999) 3.

[8] S. Dimopoulos *et al.*, Phys. Rev. Lett. **76** (1996) 3494;
S. Dimopoulos *et al.*, Nucl. Phys. **B488** (1997) 39;
S. Ambrosanio *et al.*, Phys. Rev. **D54** (1996) 5395;
S. Ambrosanio *et al.*, Phys. Rev. **D56** (1997) 1761.

[9] A. Brignole, F. Feruglio and F. Zwirner, Nucl. Phys. **B516** (1998) 13;
A. Brignole, F. Feruglio and F. Zwirner, Erratum-ibid. **B555** (1999) 653.

[10] S. Ambrosanio and B. Mele, Phys. Rev. **D52** (1995) 3900;
S. Ambrosanio and B. Mele, Phys. Rev. **D53** (1996) 2541;
S. Ambrosanio *et al.*, Nucl. Phys. **B478** (1996) 46;
S. Ambrosanio and B. Mele, Phys. Rev. **D55** (1997) 1392;
G.L. Kane and G. Mahlon, Phys. Lett. **B408** (1997) 222.

[11] J. L. Lopez *et al.*, Phys. Rev. Lett. **77** (1996) 5168;
J. L. Lopez *et al.*, Phys. Rev. **D55** (1997) 5813.

[12] DELPHI Collaboration, P. Aarnio *et al.*, Nucl. Inst. and Meth. **A303** (1991) 233;
DELPHI Collaboration, P. Abreu *et al.*, Nucl. Inst. and Meth. **A378** (1996) 57.

[13] S.J. Alvsvaag *et al.*, Nucl. Inst. and Meth. **A425** (1999) 106.

[14] DELPHI Collaboration, DELPHI 89-67 PROG 142;
DELPHI Collaboration, DELPHI 89-68 PROG 143.

[15] T.W. Anderson, An introduction to multivariate analysis, New York Wiley, 1958.

[16] T. Alderweireld, I. Gil, P. Rebecchi DELPHI 99-177 PHYS 843 PUB 1

[17] S. Jadach *et al.*, Comp. Phys. Comm. **66** (1991) 276;
S. Jadach*et al.*, Comp. Phys. Comm. **79** (1994) 503.

[18] D. Karlen, Nucl. Phys. **B289** (1987) 23.

[19] E. Falk, V. Hedberg and G. von Holtey, CERN SL/97-04(EA).

[20] G. Montagna *et al.*, Nucl. Phys. **B452** (1995) 161;
G. Montagna *et al.*, Nucl. Phys. **B541** (1999) 31.

[21] F.A. Berends *et al.* Nucl. Phys. **B61** (1973) 414;
F.A. Berends *et al.* Nucl. Phys. **B186** (1981) 22;
F.A. Berends *et al.* Nucl. Phys. **B239** (1984) 395.

[22] F.A. Berends *et al.* Nucl. Phys. **B304** (1988) 712.

[23] Z. Berezhiani, A. Rossi, DFAQ-01/TH/08 (hep-ph/0111137)

[24] S. Katsanevas and P. Morawitz, Comp. Phys. Comm. **112** (1998) 227.

[25] A.L. Read, DELPHI 97-158 PHYS 737;
E Gross, A.L. Read and D. Lellouch, Proc. of "12^e Rencontres de Physique de la Vallée d'Aoste", M Greco INFN, Frascati, 1998 Frascati physics series 12 (599-628).

[26] J. L. Lopez and D.V. Nanopoulos, Phys. Rev. **D55** (1997) 4450.

[27] The CDF collaboration, F. Abe *et al.*, Phys. Rev. Lett. **81** (1998) 1791.

	Type	Angular coverage	σ_E/E	X_0
STIC:	Lead/scint.	$2^\circ < \theta < 10^\circ$, $170^\circ < \theta < 178^\circ$	$0.0152 \oplus (0.135/\sqrt{E})$	27
FEMC:	Lead glass	$10^\circ < \theta < 37^\circ$, $143^\circ < \theta < 170^\circ$	$0.03 \oplus (0.12/\sqrt{E}) \oplus (0.11/E)$	20
HPC:	Lead/gas	$40^\circ < \theta < 140^\circ$	$0.043 \oplus (0.32/\sqrt{E})$	18

Table 1: Polar angle coverage, energy resolution (where E is in GeV and $\oplus$ denotes addition in quadrature) and thickness (in radiation lengths) of the electromagnetic calorimeters in DELPHI.

Year	$\sqrt{s}$ (GeV)		Luminosity (pb)		
	bin	average	HPC	FEMC	STIC
1997	180.8-184.0	182.7	50.2	49.2	51.4
1998	188.3-189.2	188.6	154.7	157.7	157.3
1999	191.4-191.8	191.6	25.9	25.9	25.9
1999	195.4-195.9	195.5	76.4	76.4	76.4
1999	199.1-200.0	199.5	83.4	83.4	83.4
1999	201.4-202.0	201.6	40.6	40.6	40.6
2000	202.0-204.5	203.7	8.4	8.4	8.4
2000	204.5-206.0	205.2	76.2	76.3	76.1
2000	206.0-207.5	206.7	121.6	125.7	125.6
2000	207.5-209.2	208.2	8.3	8.4	8.4

Table 2: The different datasets used in the single photon analysis.

	$\sqrt{s}$	180-190 GeV	190-200 GeV	200-210 GeV
	$<\sqrt{s}>$	187.2 GeV	196.8 GeV	205.4 GeV
STIC	$N_{observed}$:	126	90	114
	$N_{background}$:	10.1	7.2	7.1
$0.3 < x_\gamma < 0.9$	$N_{e^+e^-\to\nu\bar{\nu}\gamma}$:	123.8±1.2	86.9±1.0	112.9±1.7
$3.8^\circ < \theta_\gamma < 8^\circ$	σ_{meas} (pb)	1.37±0.14	1.22±0.14	1.12±0.11
$172^\circ < \theta_\gamma < 176.2^\circ$	$\sigma_{\nu\bar{\nu}\gamma(\gamma)}$ (pb)	1.44	1.29	1.18
	N_ν	2.83±0.31	2.81±0.37	2.81±0.33
FEMC	$N_{observed}$:	220	175	224
	$N_{background}$:	9.5	8.9	9.0
$0.2 < x_\gamma < 0.9$	$N_{e^+e^-\to\nu\bar{\nu}\gamma}$:	208.3±2.2	168.1±1.1	200.4±1.6
$12^\circ < \theta_\gamma < 32^\circ$	σ_{meas} (pb)	1.98±0.14	1.71±0.14	1.71±0.12
$148^\circ < \theta_\gamma < 168^\circ$	$\sigma_{\nu\bar{\nu}\gamma(\gamma)}$ (pb)	1.89	1.76	1.61
	N_ν	3.03±0.25	2.90±0.28	3.30±0.27
HPC	$N_{observed}$:	177	127	190
	$N_{background}$:	0.3	0.2	0.1
$x_\gamma > 0.06$	$N_{e^+e^-\to\nu\bar{\nu}\gamma}$:	190.1±2.6	151.4±1.1	198.1±2.0
$45^\circ < \theta_\gamma < 135^\circ$	σ_{meas} (pb)	1.74±0.13	1.37±0.12	1.47±0.11
	$\sigma_{\nu\bar{\nu}\gamma(\gamma)}$ (pb)	1.97	1.75	1.57
	N_ν	2.67±0.28	2.08±0.29	2.61±0.30

Table 3: The number of selected and expected single photon events and the measured and calculated cross-section with the three calorimeters for $e^+e^- \to \nu\bar{\nu}\gamma(\gamma)$ (KORALZ with three neutrino generations) and the number of neutrino generations calculated from the cross-sections. The errors are statistical only.

	HPC		FEMC		STIC	
Source	Variation	$\Delta\sigma$	Variation	$\Delta\sigma$	Variation	$\Delta\sigma$
Luminosity	$\pm$0.6%	$\pm$0.6%	$\pm$0.6%	$\pm$0.6%	$\pm$0.6%	$\pm$0.6%
Trigger efficiency	$\pm$5%	$\pm$5%	$\pm$2%	$\pm$2%	$\pm$6%	$\pm$6%
Identification efficiency	$\pm$5%	$\pm$5%	$\pm$6%	$\pm$6%	$\pm$5%	$\pm$5%
Calorimeter energy scale	$\pm$5%	$\pm$4%	$\pm$4%	$\pm$4%	$\pm$0.5%	$\pm$1%
Background	$\pm$57%	$\pm$0.1%	$\pm$55%	$\pm$2%	$\pm$62%	$\pm$5%
Total		$\pm$8%		$\pm$8%		$\pm$9%

Table 4: Contributions to systematic error. The total systematic error is the quadratic sum of the individual errors.

	204-209 GeV		130-209 GeV	
	Observed	Expected	Observed	Expected
Preselected multi-photon events	18	19.8$\pm$0.6	68	64.6$\pm$1.3
$e^+e^- \to \tilde{\chi}_1^0\tilde{\chi}_1^0 \to \tilde{G}\gamma\tilde{G}\gamma$ selection	8	7.3$\pm$0.4	24	20.9$\pm$0.7
$e^+e^- \to \tilde{\chi}_2^0\tilde{\chi}_2^0 \to \tilde{\chi}_1^0\gamma\tilde{\chi}_1^0\gamma$ selection	9	7.9$\pm$0.4	26	23.8$\pm$0.8
Non-pointing single-photon events	5	3.0	16	14.6

Table 5: The number of observed and expected events from Standard Model sources in four selected data samples.

Dimensions	σ_{Limit} (pb)	M_D (expected)	M_D (obtained)	Radius
2	0.14	>1.32 TeV	>1.36 TeV	<0.26 mm
3	0.14	>1.01 TeV	>1.05 TeV	<3.3 nm
4	0.14	>0.82 TeV	>0.84 TeV	<13 pm
5	0.17	>0.69 TeV	>0.69 TeV	<0.48 pm
6	0.18	>0.59 TeV	>0.59 TeV	<54 fm

Table 6: Limits at the 95% confidence level on the fundamental mass scale M_D and the radius for different numbers of extra dimensions. Note that the definition of M_D in [6] is a factor $2^{1/(n-2)}$ smaller than in [7] and that the limits presented here is for an M_D as defined by [7].

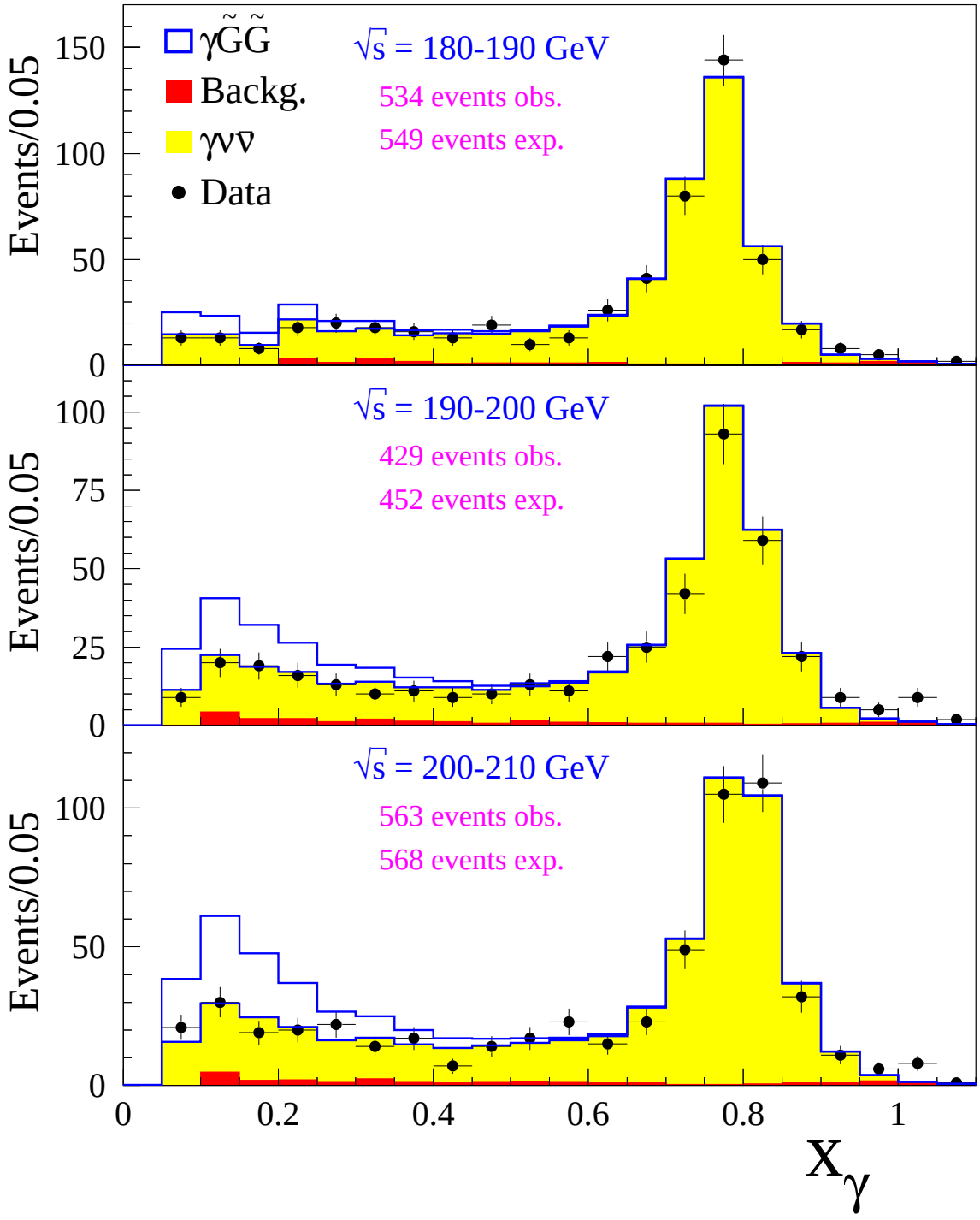

Figure 1: x_γ of selected single photons for three $\sqrt{s}$-bins. The light shaded area is the expected distribution from $e^+e^- \to \nu\bar{\nu}\gamma$ and the dark shaded area is the total background from other sources. Indicated in the plot is also the expected signal from $e^+e^- \to \tilde{G}\tilde{G}\gamma$ under the assumption that $m_{\tilde{G}} = 7 \cdot 10^{-6}$ eV/c^2.

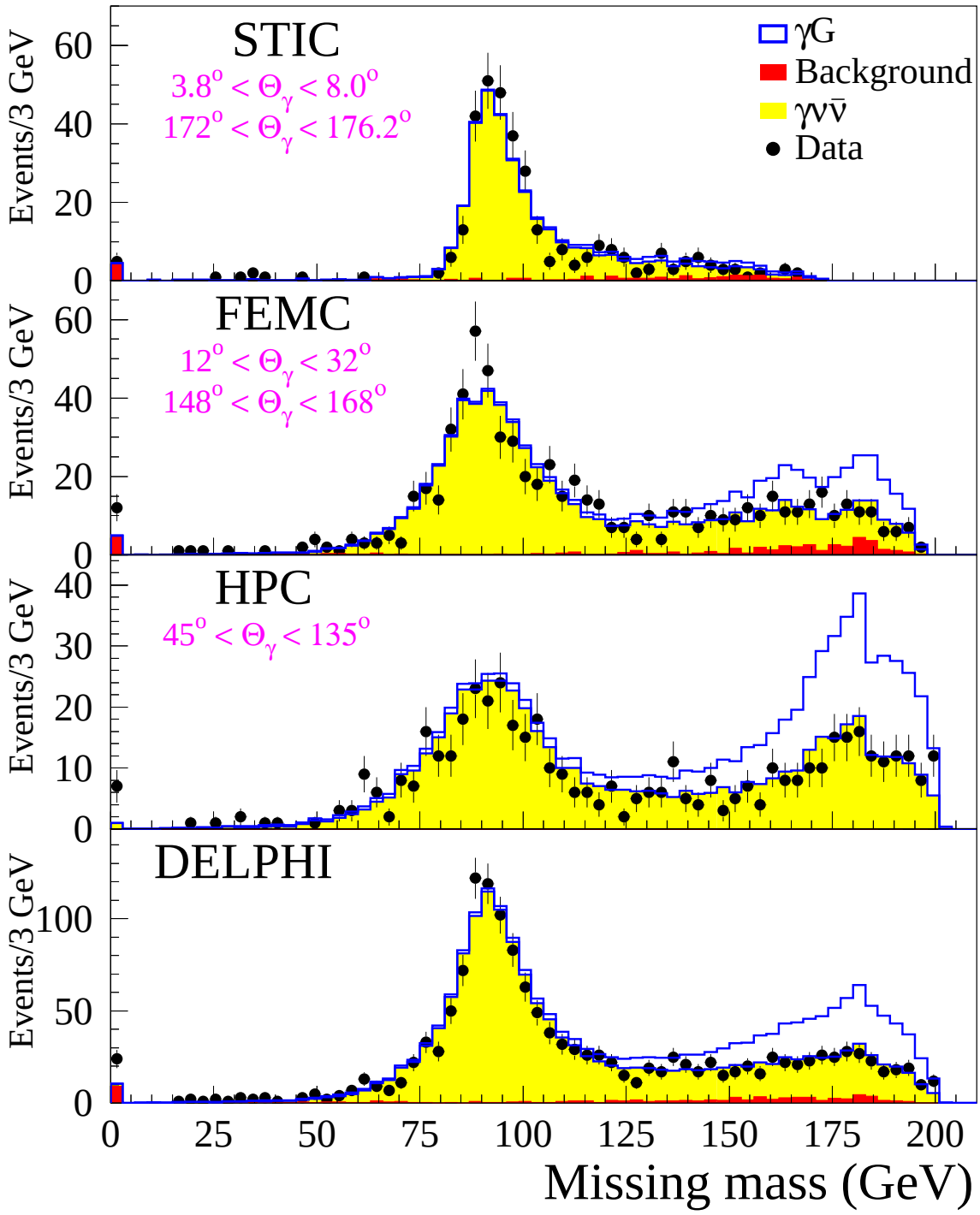

Figure 2: Missing mass (or recoil mass) distributions of all single photon events in DELPHI (from data recorded at $\sqrt{s} = 181$-209 GeV). The figure shows the missing mass distribution from each calorimeter separately and the bottom plot shows the combined spectrum. The light shaded area is the expected distribution from $e^+e^- \to \nu\bar{\nu}\gamma$ and the dark shaded area is the total background from other sources. The expected signal from $e^+e^- \to \gamma G$ production is indicated (two extra dimensions and $M_D = 0.75$ TeV was assumed in this calculation).

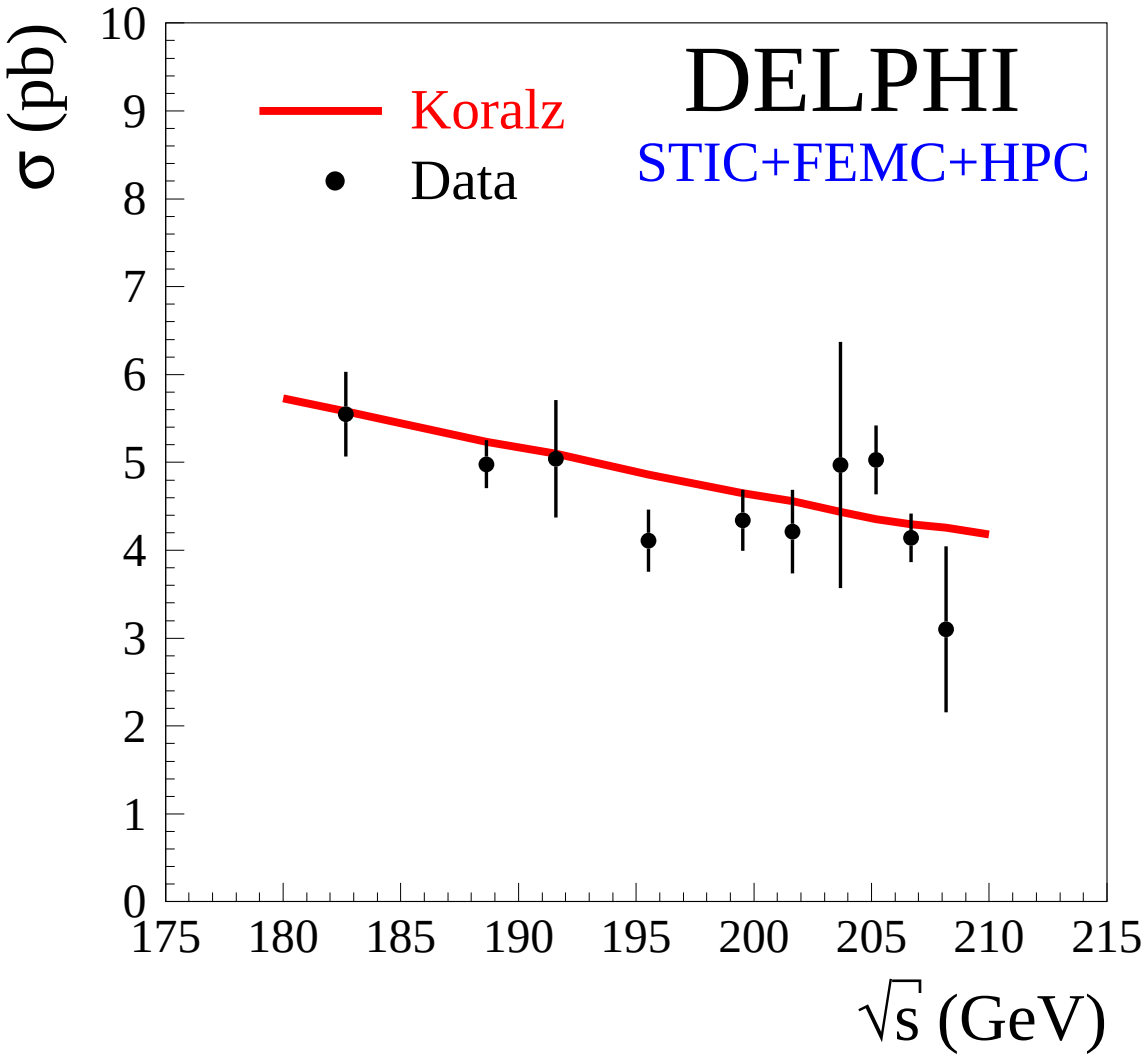

Figure 3: The single photon cross-section measured by the STIC, FEMC and HPC detectors compared to the cross-section predicted by Koralz.

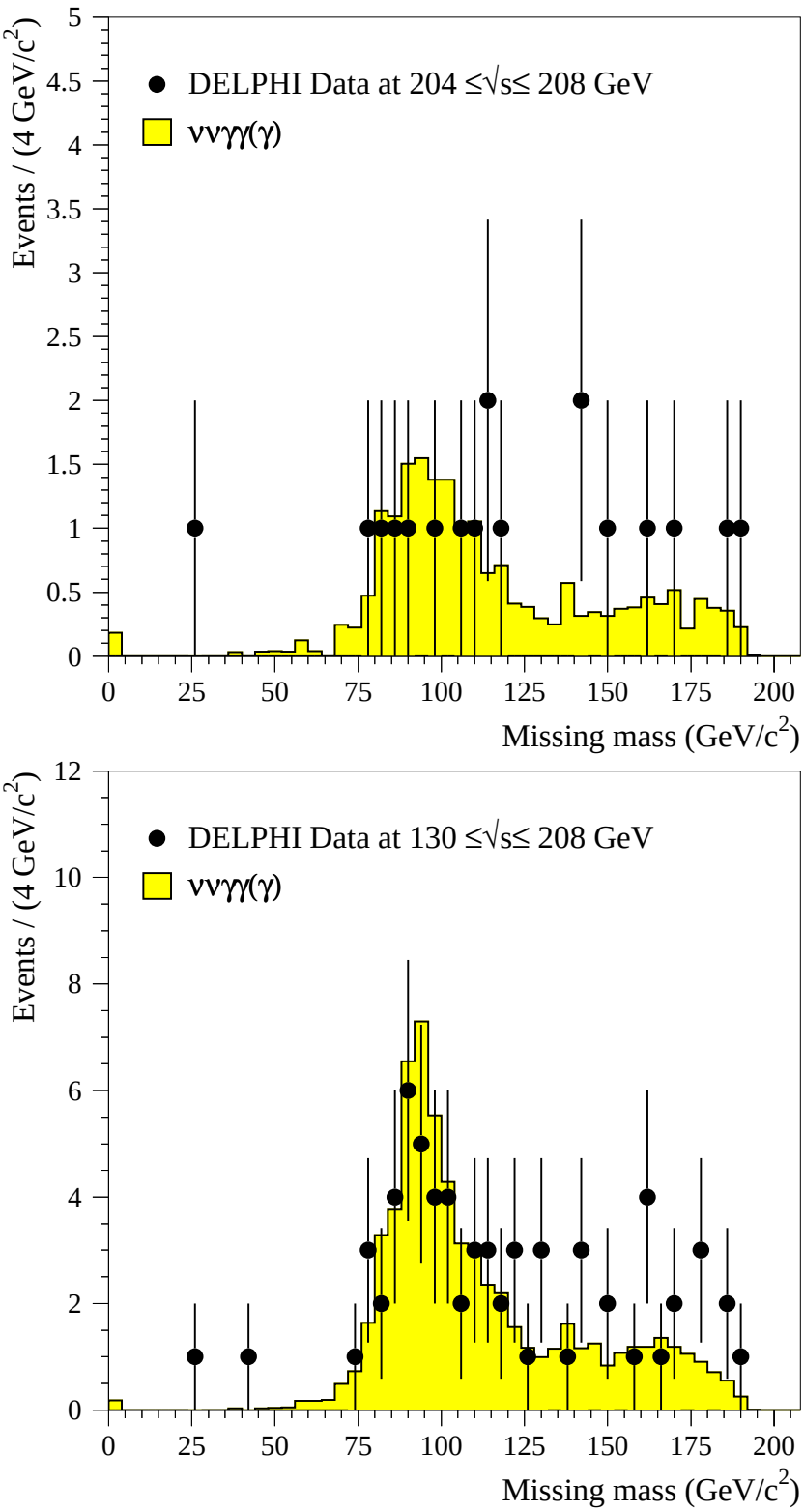

Figure 4: Missing mass distribution observed after multi-photon preselection in the 204-209 GeV sample (top) and the combined 130-209 GeV sample (bottom).

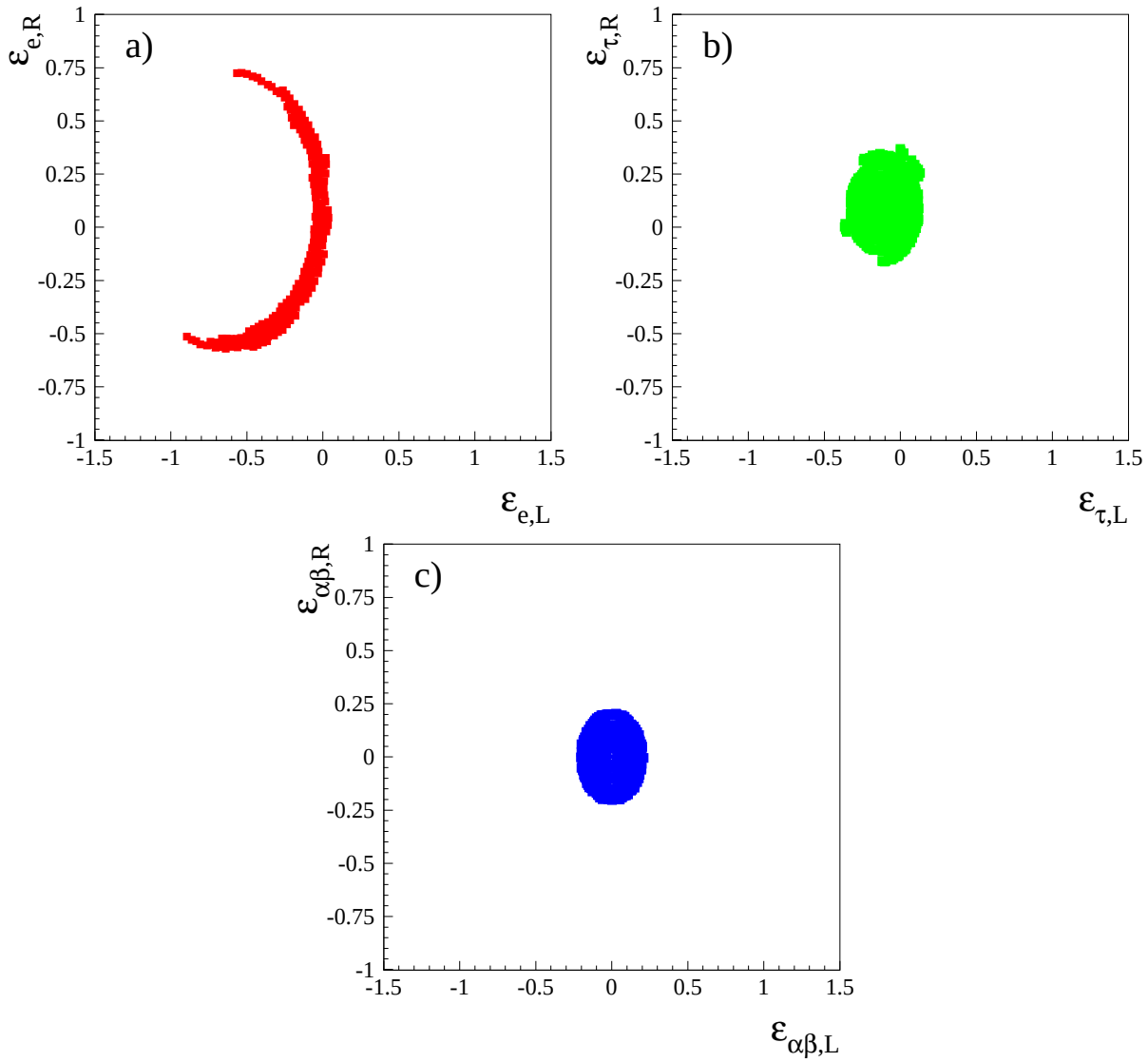

Figure 5: a) The region in the $\epsilon_{eL} - \epsilon_{eR}$ plane which is not excluded. b) The region in the $\epsilon_{\tau L} - \epsilon_{\tau R}$ plane which is not excluded. c) The region in the $\epsilon_{\alpha\beta L} - \epsilon_{\alpha\beta R}$ ($\alpha \neq \beta$) plane which is not excluded.

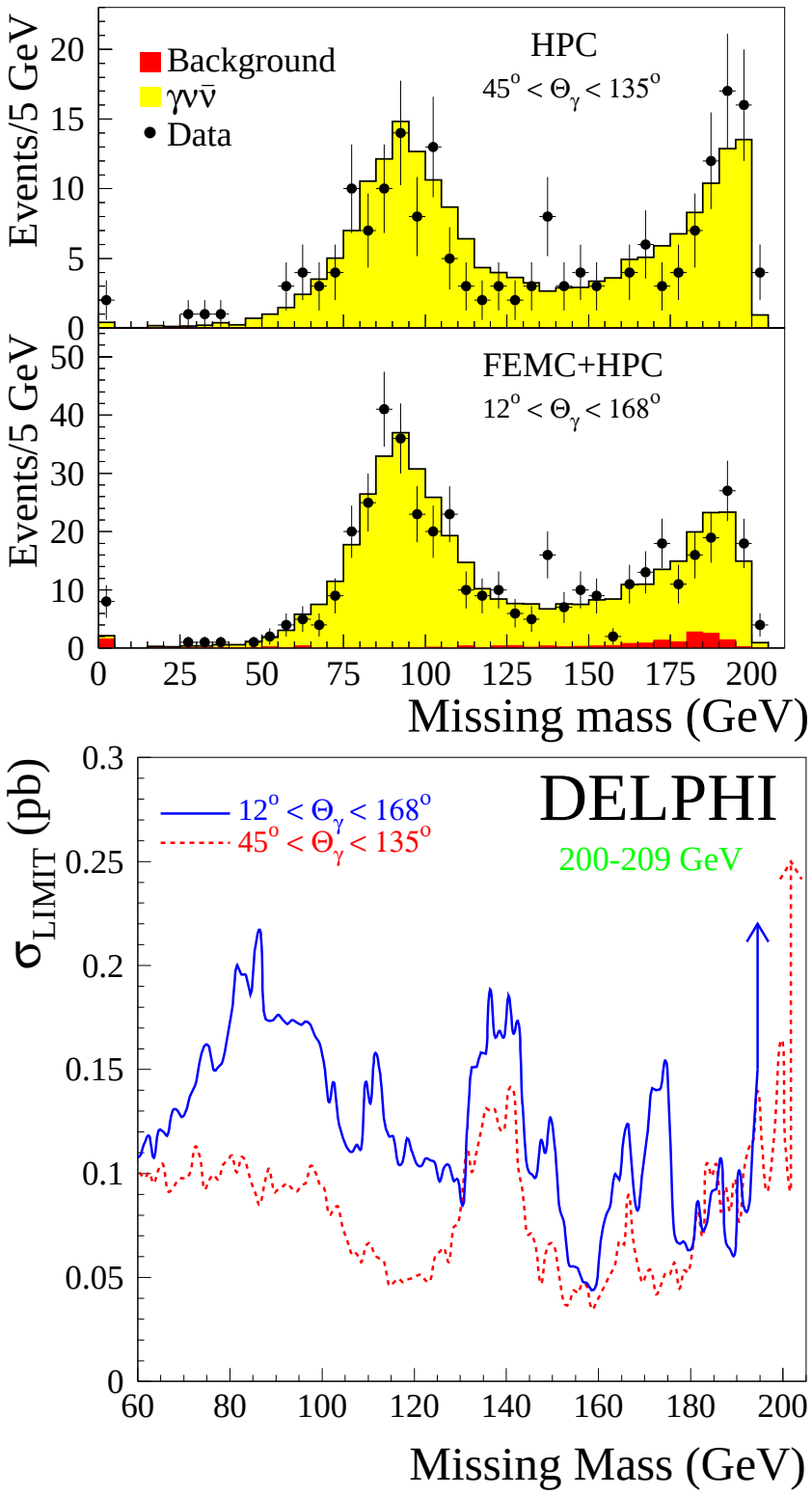

Figure 6: Top: The distributions of the missing mass for the events at 200-209 GeV in the HPC and in the FEMC+HPC. The light shaded area is the expected distribution from $e^+e^- \to \nu\bar{\nu}\gamma$ and the dark shaded area is the total background from other sources. Bottom: upper limit at 95% C.L. (within the solid angles described) for the production of a new unknown stable neutral object .

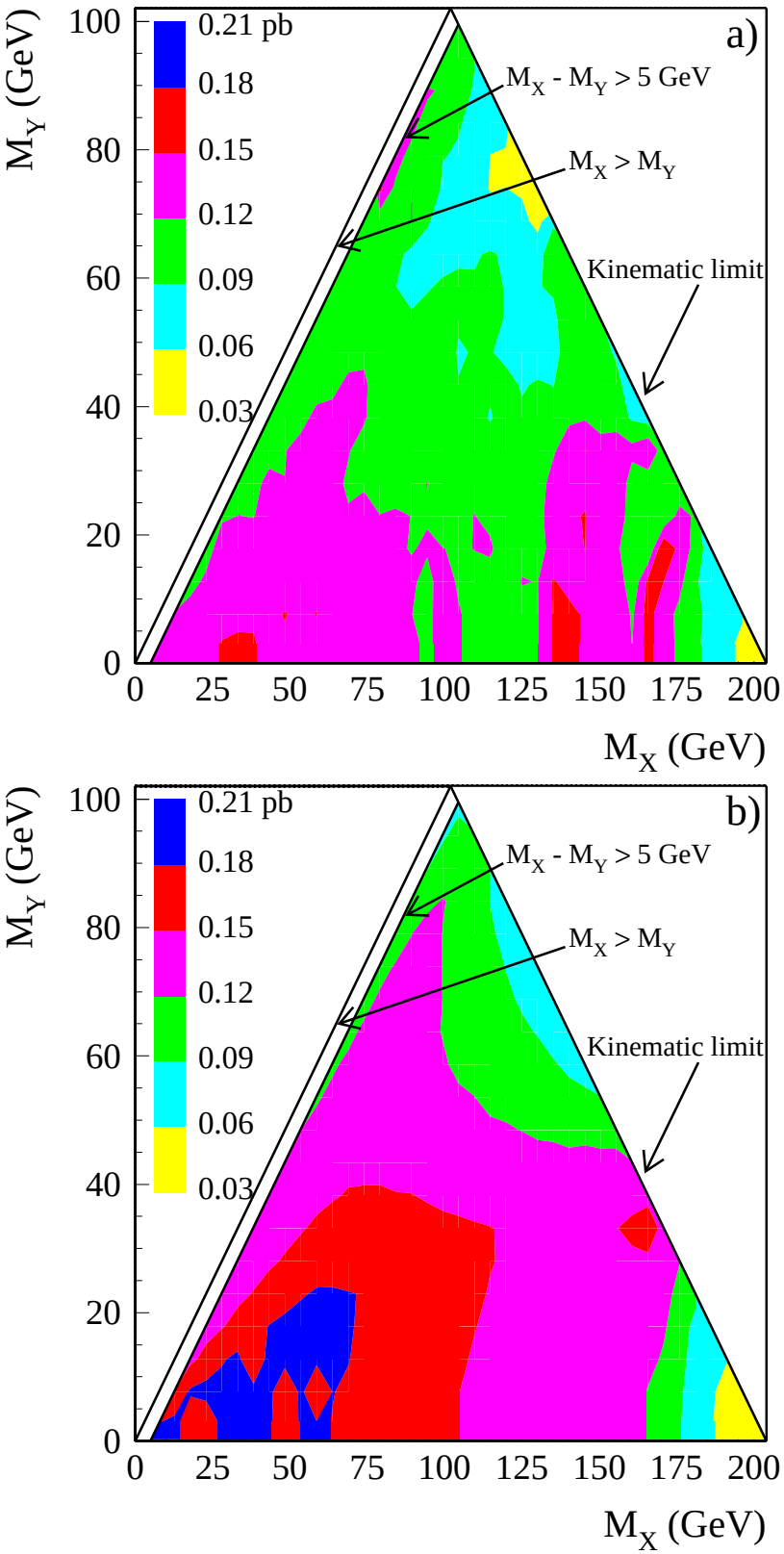

Figure 7: The obtained (a) and expected (b) cross section limit at 95% C.L. and at 205 GeV for the process $e^+e^- \to XY \to YY\gamma$ where X and Y are hypothetical new neutral particles.

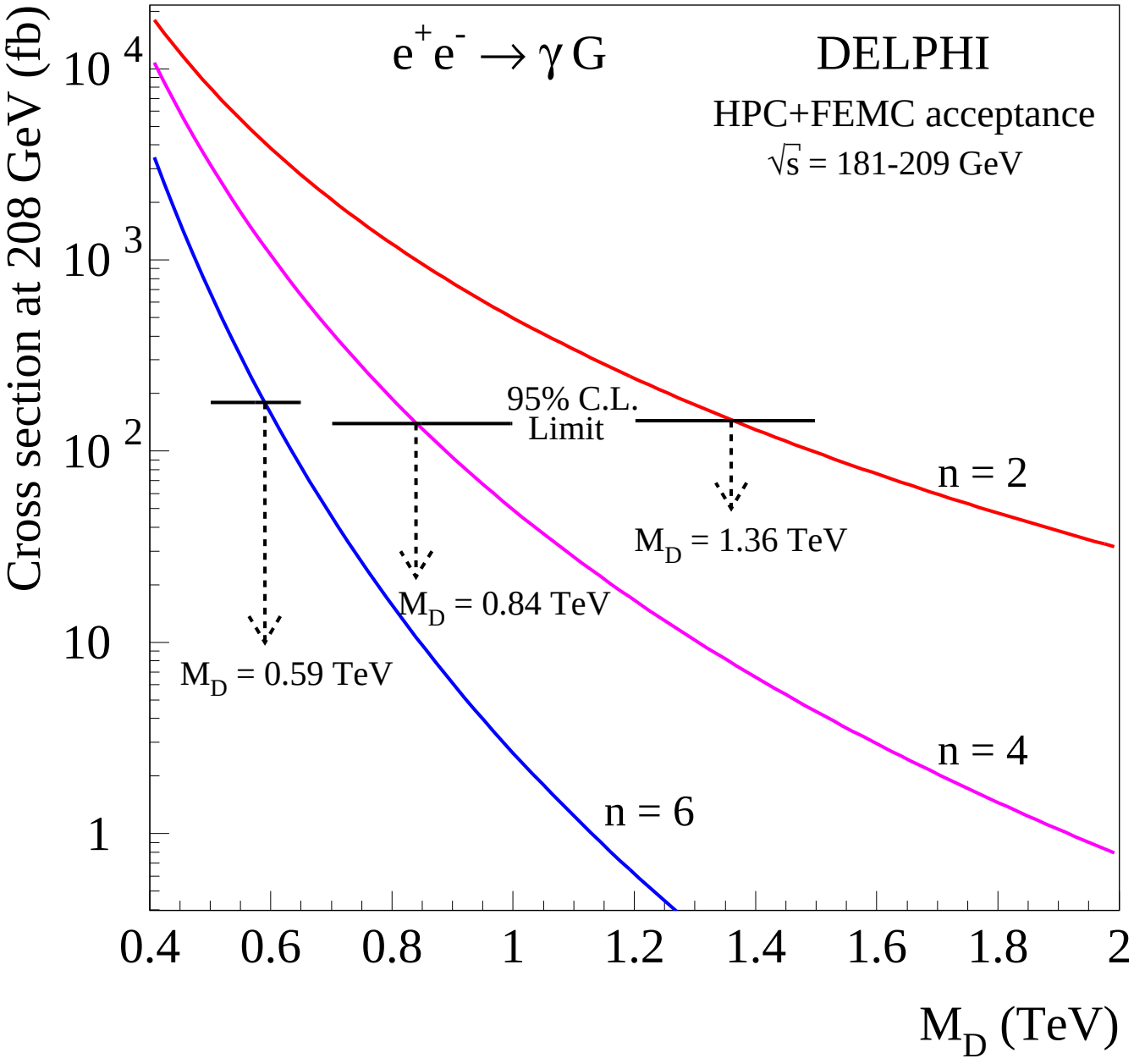

Figure 8: The cross-section limit at 95% C.L. for $e^+e^- \to \gamma G$ production at $\sqrt{s}$=208 GeV and the expected cross-section for 2, 4 and 6 extra dimensions.

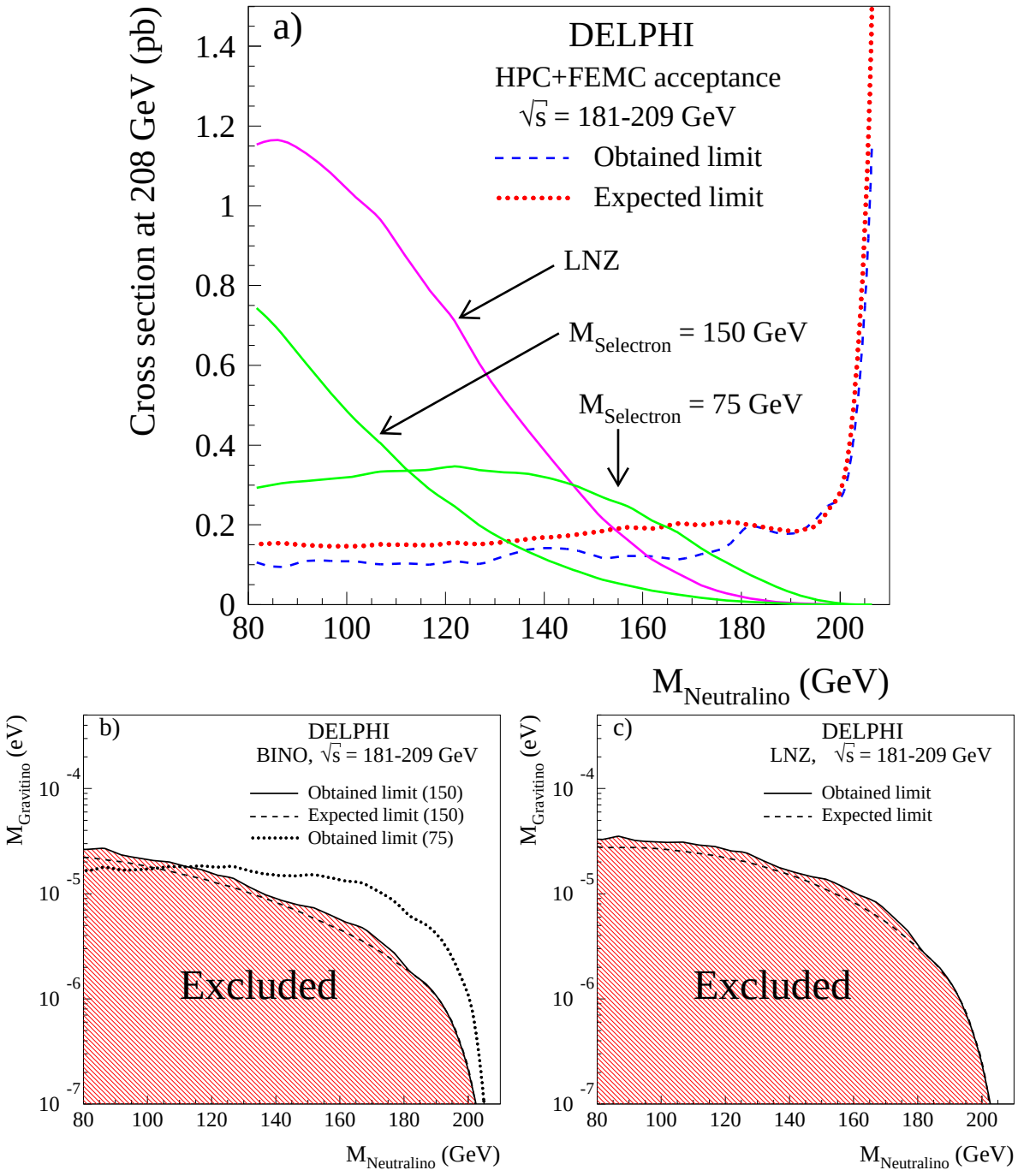

Figure 9: a) Cross section limit at 95% C.L. and at $\sqrt{s}$ =208 GeV of the process $e^+e^- \rightarrow \tilde{G}\tilde{\chi}_1^0 \rightarrow \tilde{G}\tilde{G}\gamma$ as a function of the $\tilde{\chi}_1^0$ mass. The predicted cross-sections under the assumption that the neutrino is a Bino or as described by the LNZ-model are also shown for $m_{\tilde{G}} = 1 \times 10^{-5}$ GeV. b), c) Exclusion plots in the $m_{\tilde{\chi}_1^0}$-$m_{\tilde{G}}$ mass plane.

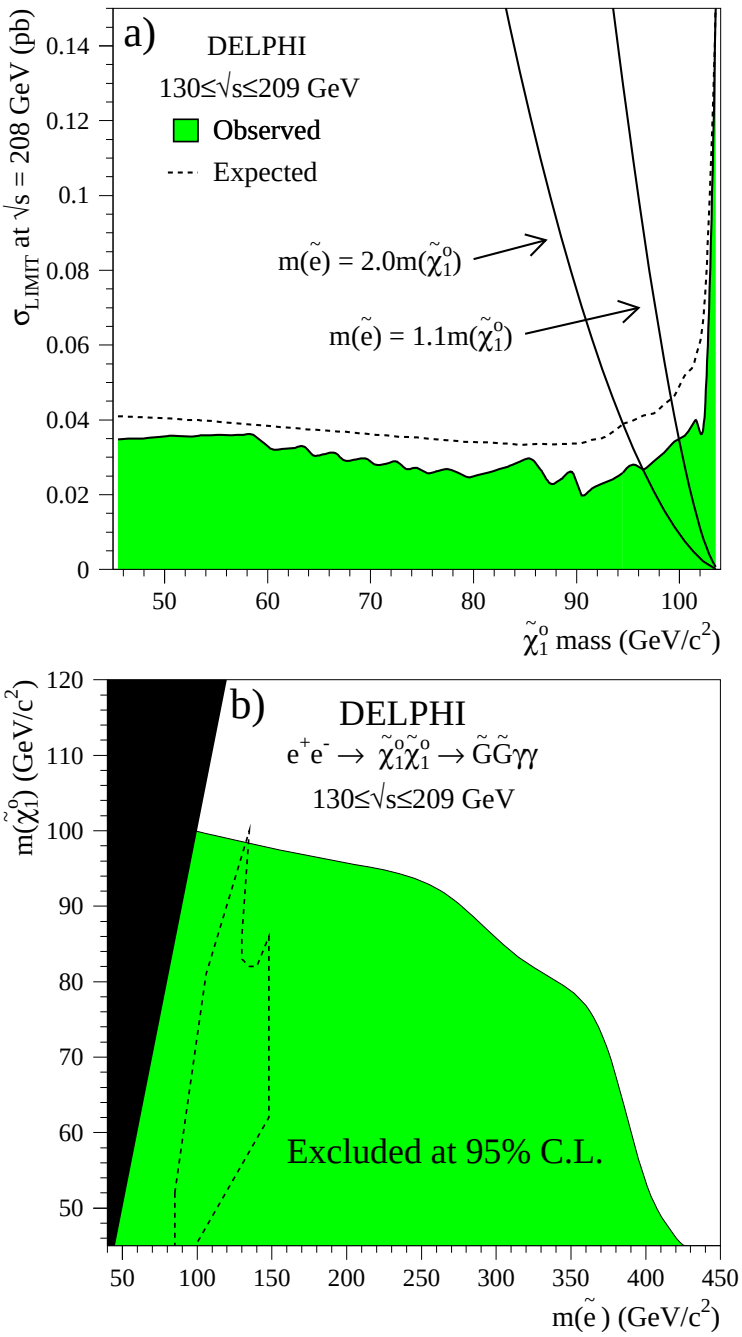

Figure 10: a) Upper limit at 95% C.L. on the cross-section at $\sqrt{s}$ =208 GeV of the process $e^+e^- \to \tilde{\chi}_1^0\tilde{\chi}_1^0 \to \tilde{G}\gamma\tilde{G}\gamma$ as a function of the $\tilde{\chi}_1^0$ mass and the predicted cross-section for two different assumptions for the selectron mass. The limit was obtained by combining all data taken at $\sqrt{s}$ =130-209 GeV, assuming the signal cross-section scales as β/s (where β is the neutralino velocity). b) The shaded area shows the exclusion region in the $m_{\tilde{\chi}}$ versus $m_{\tilde{e}_R}$ plane, calculated from the DELPHI data at $\sqrt{s}$ =130-209 GeV. The region compatible with the selectron interpretation [26] of the CDF ee$\gamma\gamma$ event [27] is shown by the dashed line.

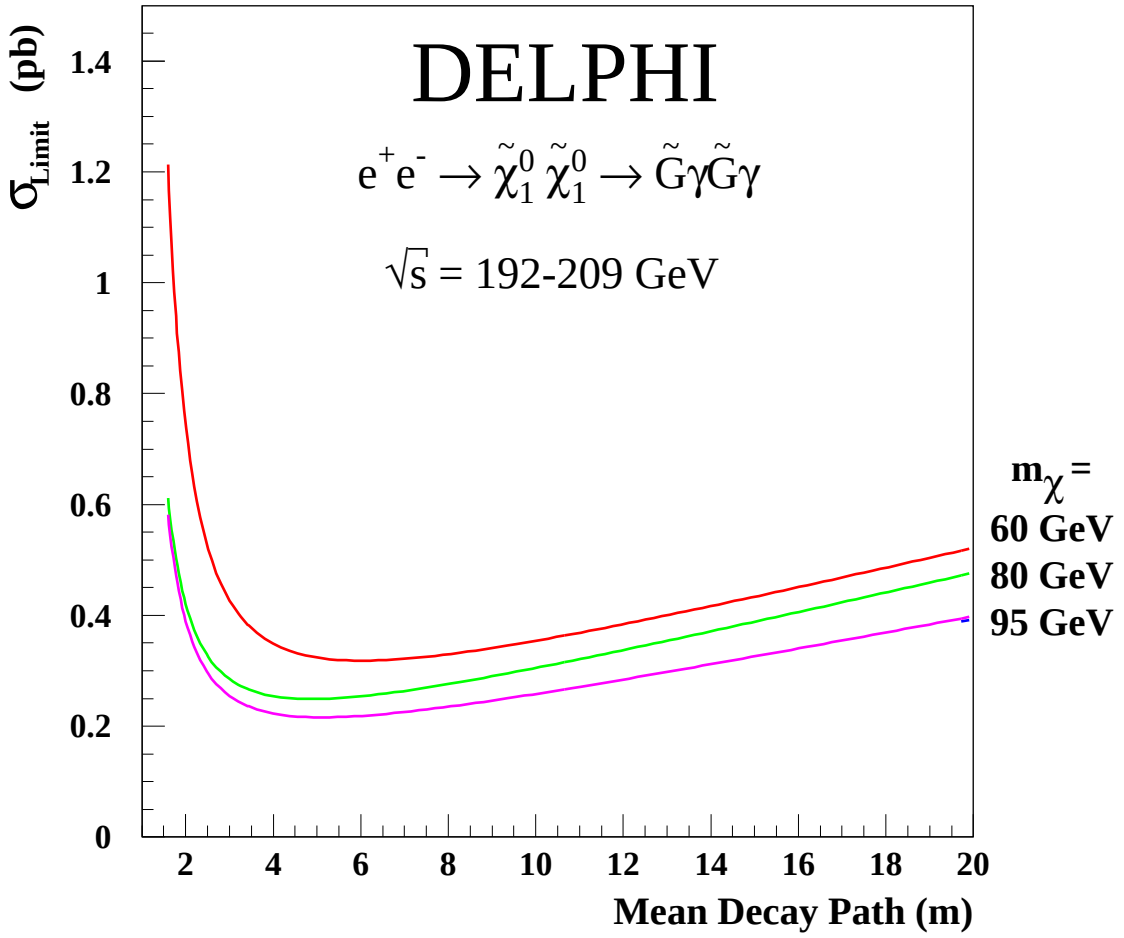

Figure 11: Upper limit at 95% C.L. on the cross-section of the process $e^+e^- \to \tilde{\chi}_1^0\tilde{\chi}_1^0 \to \tilde{G}\gamma\tilde{G}\gamma$ as a function of the $\tilde{\chi}_1^0$ mean decay path for different hypotheses for the neutralino mass. The data collected at $\sqrt{s}$ =192-209 GeV was used to produce this plot.

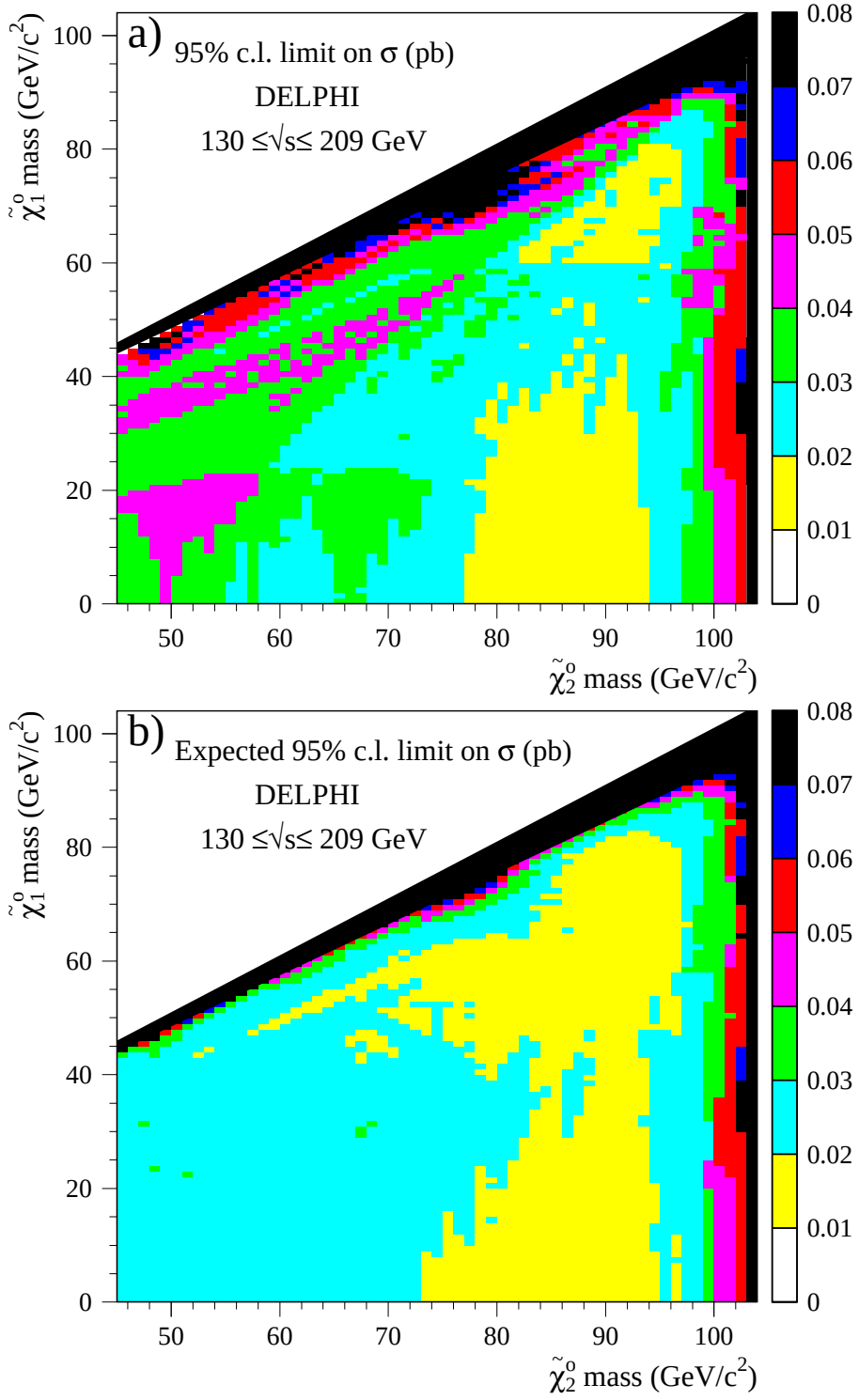

Figure 12: a) The observed upper limit at 95% C.L. on the cross-section at $\sqrt{s}$ =208 GeV of the process $e^+e^- \to \tilde{\chi}_2^0\tilde{\chi}_2^0 \to \tilde{\chi}_1^0\gamma\tilde{\chi}_1^0\gamma$ as a function of the $\tilde{\chi}_1^0$ and the $\tilde{\chi}_2^0$ mass. The different shaded areas correspond to limits in pb as indicated by the shading scale on the right hand side. The limit was obtained by combining the data taken at $\sqrt{s}$ =130-209 GeV, assuming the signal cross-section to scale as β/s. b) The expected upper limit at 95% C.L. on the cross-section at $\sqrt{s}$ =208 GeV of the process $e^+e^- \to \tilde{\chi}_2^0\tilde{\chi}_2^0 \to \tilde{\chi}_1^0\gamma\tilde{\chi}_1^0\gamma$.